Hindawi
International Journal of Corrosion
Volume 2021, Article ID 6695299, 13 pages
https://doi.org/10.1155/2021/6695299

Research Article

Use of a Metallic Complex Derived from Curcuma Longa as Green Corrosion Inhibitor for Carbon Steel in Sulfuric Acid

E. A. Florez-Frias,[1] V. Barba,[2] R. Lopez-Sesenes,[3] L. L. Landeros-Martínez,[4] J. P. Flores-De los Ríos,[5] M. Casales,[6] and J. G. Gonzalez-Rodriguez[1]

[1]*Universidad Autonoma del Estado de Morelos, CIICAp, Av. Universidad 1001-62209, Cuernavaca, Morelos, Mexico*
[2]*Universidad Autonoma del Estado de Morelos, CIQ, Av. Universidad 1001-62209, Cuernavaca, Morelos, Mexico*
[3]*Universidad Autonoma del Estado de Morelos, FCQeI, Av. Universidad 1001-62209, Cuernavaca, Morelos, Mexico*
[4]*Universidad Autónoma de Chihuahua, Facultad de Ciencias Químicas, Circuito No. 1, Campus Universitario 2, Chihuahua, Chihuahua C.P. 31125, Mexico*
[5]*Universidad Autónoma de Chihuahua, Facultad de Ingeniería, Circuito No. 1, Campus Universitario 2, Chihuahua, Chihuahua C.P. 31125, Mexico*
[6]*Universidad Nacional Autónoma de Mexico, Av. Universidad S/N 62209, Cuernavaca, Morelos, Mexico*

Correspondence should be addressed to J. G. Gonzalez-Rodriguez; ggonzalez@uaem.mx

Received 19 October 2020; Revised 21 December 2020; Accepted 5 January 2021; Published 18 January 2021

Academic Editor: Michael I. Ojovan

Copyright © 2021 E. A. Florez-Frias et al. This is an open access article distributed under the Creative Commons Attribution License, which permits unrestricted use, distribution, and reproduction in any medium, provided the original work is properly cited.

A tin-containing metallic complex derived from *Curcuma longa*, bis[1,7-bis(4-hydroxy-3-methoxyphenyl)-1,6-heptadiene-3,5-dionato-κO,κO$'$]bis(butyl), has been obtained and used as a green corrosion inhibitor for carbon steel in 0.5 M sulfuric acid by using weight loss, electrochemical techniques, and the Density Functional Theory. It was found that the obtained metallic complex greatly decreases the steel corrosion rate by adsorption according to a Frumkin model in a weak, physical type of adsorption. Inhibitor efficiency increased with its concentration, and it acted as a mixed type of inhibitor. Results were supported by quantum-chemical research in order to examine the relationship between structural and electronic properties and the inhibitor efficiency.

1. Introduction

The use of organic inhibitors, those which contain oxygen, nitrogen, sulfur, or carbon, is one of the most commonly used methods to combat the corrosion of metals, which causes huge economic loses and severe accidents in the industry [1–6]. This is because compounds with π-bonds generally exhibit good inhibitive properties due to their interaction with the metal surface [7–9]. The way they decrease the corrosion rate is by the formation of a compact barrier onto the metal surface by adsorbing on the metal surface and blocking the active sites by displacing water molecules. However, organic inhibitors are toxic, highly expensive, and environmentally unfriendly. Thus, many efforts have been made in the last few years towards the use of compounds found in plants including seeds, roots, flowers, etc. since they contain phytochemical compounds which incorporate effective corrosion inhibitors [10–17].

Curcumin is one of the main phenolic compounds present in the *Curcuma longa* rhizome which has been used in Asia since ancient times. The powder obtained from the rhizome of *Curcuma longa* has many uses including as a spice, food colouring, and preservative, among others. In addition to India, it is also cultivated in China, Japan, and Burma. The obtained powder from *Curcuma longa* has a peppery bitter flavour and is the main ingredient to make the spice known worldwide as curry [18–21]. Due to the potent antioxidants contained in *Curcuma longa*, it is used in folk Indian

medicine to help combat illness such as digestive problems and fever and reduce cholesterol, and recently, some anti-Alzheimer, antimutagenic, anticarcinogenic, antimicrobial, and antiviral qualities have been found.

Curcuma longa extract has been used as a corrosion inhibitor for steel in different environments due to the presence of antioxidants [22–25]. Alternatively, since curcumin is the most abundant compound found in *Curcuma longa*, some of its derivatives have also been evaluated as green and ecofriendly corrosion inhibitors for metals because of the existence of inhibition aromatic rings which block the active surface sites to reduce the corrosion of steel in corrosive solutions [26–29]. For instance, Fouda and Elattar [26] evaluated three curcumin derivatives, namely, 1,7-bis-(4-hydroxy-3-methoxy-phenyl)-hepta-1,6-diene-4-arylazo-3,5-dione (I-V), as green corrosion inhibitors for brass in 2.0 M nitric acid by using weight loss and electrochemical measurements. They found that these curcumin derivatives had a corrosion efficiency which increased with their concentration but decreased with an increase in the testing temperature. In another research work [27], Rajendran et al. evaluated the corrosion inhibition efficiency for pure aluminium in artificial sea water solution by using weight loss tests and potentiodynamic polarization curves. Their results showed that the curcumin corrosion efficiency was as high as 98% and the corrosion current density value, I_{corr}, was decreased by one order of magnitude. Finally, Kandias et al. evaluated different curcuminoids extracted from *Curcuma longa* as green corrosion inhibitors for carbon steel in 1.0 M sodium chloride solution by using gravimetric and electrochemical tests [28]. They found that the curcuminoid corrosion efficiency increased with their concentration, bringing a reduction in the I_{corr} value from 180 to 34 μA/cm^2. Thus, the goal of this work is to evaluate the use of a new curcumin derivative as a green corrosion inhibitor for 1018 carbon steel in 0.5 M sulfuric acid solution. The reason for this is the high corrosion rates found in the metallic components, made mainly from carbon steel, in the pickling and decaling industry, where acids such as nitric, hydrochloric, and sulfuric are widely used and the use of corrosion inhibitors is compulsory.

2. Materials and Methods

2.1. Inhibitor Synthesis. The inhibitor used was bis[1,7-bis(4-hydroxy-3-methoxyphenyl)-1,6-heptadiene-3,5-dionato-κO,κO$'$]bis(butyl), a Sn-containing metallic complex derived from curcumin. The synthesis procedure started with the curcumin obtained from *Curcuma longa* bulbs described elsewhere [29]. Briefly, *Curcuma longa*, which was purchased from a local market, was dissolved in ethanol (1 L). The solvent was removed by using an evaporator, then the solid was recrystallized in ethanol (80 mL); in the end, it was filtered to obtain an orange-red solid which was dried completely. Once the curcumin was obtained (Figure 1), 0.6 g (1.62 mmol) of curcumin was dissolved in 25 mL of methanol and stirred into a ball flask, and after this, 0.2 g (0.80 mmol) of dibutyltin oxide was added. Following this, and after the complete material dissolution (approximately 15 minutes), the reaction was carried out under reflux during 7 hours. After this, the mixture was allowed to cool down, and a red solid, metallic complex was obtained by complete evaporation of the solvent. The metallic complex characterization was made through three spectroscopic techniques including Infrared, ^{1}H Nuclear Magnetic Resonance, and Mass Spectrometry as detailed in [29]. According to Priyadarsini, this metallic complex is soluble in organic compounds, but insoluble in water or in sulfuric acid [30].

2.2. Testing Material. The testing material included AISI 1018 carbon steel containing, in wt. %, Fe-0.14, C-0.90, Mn-0.30, and S-0.30 P, which were purchased as 6.00 mm diameter rods.

2.3. Testing Solution. As testing solution, 0.5 M sulfuric acid (H_2SO_4) was prepared by using analytical grade reagents. For the weight loss tests, specimens were exposed to this electrolyte containing different concentrations of inhibitor during an exposure time of 72 hours by triplicate at room temperature, i.e., 25°C. After this, specimens were cleaned to remove the corrosion products and to obtain the weight loss per unit area, ΔW. For this, the following expression was used:

$$\Delta W = \frac{m_1 - m_2}{A}, \quad (1)$$

were m_1 is the weight of the specimen corroded in the absence of the inhibitor, m_2 is the weight of the specimen corroded in the presence of the inhibitor, and A the exposed area of the specimen. Inhibitor efficiency, I.E., was obtained as follows:

$$\text{I.E.}(\%) = \frac{\Delta W_1 - \Delta W_2}{\Delta W_1} \times 100, \quad (2)$$

where ΔW_1 is the weight loss of the specimen without inhibitor and ΔW_2 is the weight loss with inhibitor. Selected corroded specimens were observed in a low vacuum scanning electronic microscope (SEM).

2.4. Electrochemical Techniques. Specimens measuring 6.00 mm in length were cut and encapsulated in commercial polymeric resin, abraded with 600-grade emery paper, washed, and degreased with acetone. Employed electrochemical techniques included potentiodynamic polarization curves and electrochemical impedance spectroscopy (EIS). For this, a three-electrode electrochemical glass cell was used with a saturated calomel electrode (SCE) and a graphite rod as the reference and auxiliary electrodes, respectively. Before starting the experiments, specimens were immersed into the solution during an exposure time of 20 minutes to allow the free corrosion potential value, E_{corr}, to reach a steady state. For polarization curves, scanning started in a potential value of 800 which is more cathodic than the E_{corr} value, and it was scanned in the anodic direction at a scan rate of 1 mV/s up to a potential value of 400 mV which is more anodic than E_{corr}. An ACM potentiostat was used for this purpose. Corrosion current density values, I_{corr}, were calculated by using the

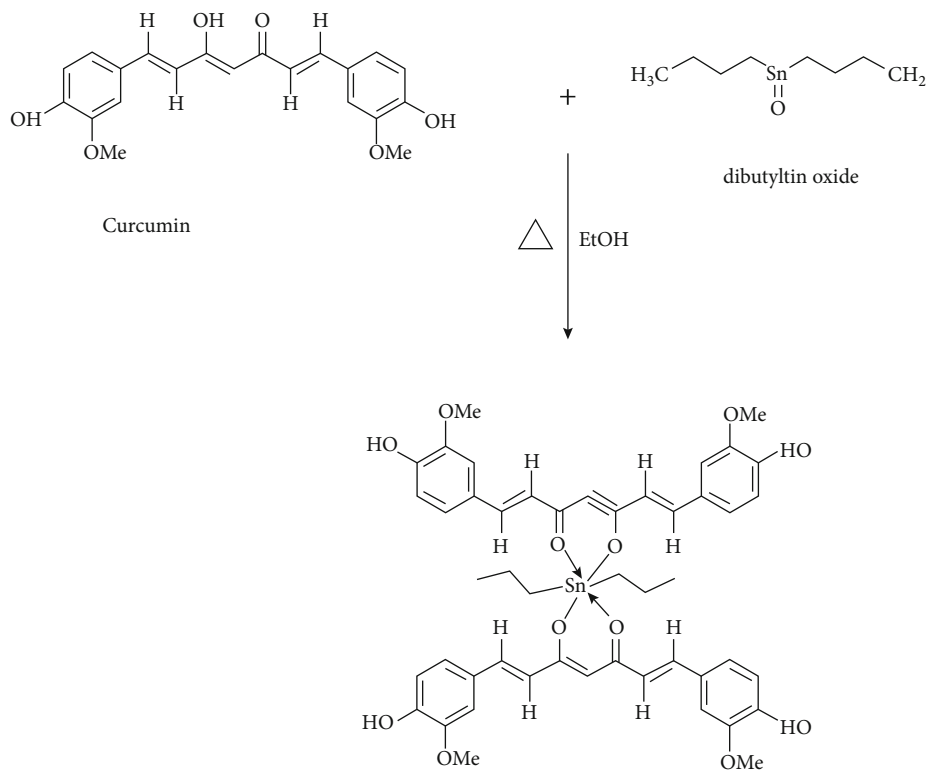

Figure 1: Scheme showing the used procedure for the synthesis of the metallic complex used as corrosion inhibitor.

Tafel extrapolation method. EIS measurements were carried out at the E_{corr} value by applying a perturbation signal with an amplitude of 15 mV peak to peak in a frequency interval of 0.01-20,000 Hz. In this case, a PC4 300 Gamry potentiostat was used.

2.5. Theoretical Calculations. Quantum calculations have been performed to try to correlate inhibitor efficiency with its electronic properties as described elsewhere [31]. All calculations were performed by using the Gaussian 09 software [31] and the Density Functional Theory (DFT) [32–40]. Parameters of interest included global hardness (η) [41], electronegativity (χ) [42], electrophilicity (ω) [43], dipolar moment (μ) [44], and the Highest Occupied Molecular Orbital (HOMO) and Lower Unoccupied Molecular Orbital (LUMO) [34–44]. In addition to these parameters, Fukui functions were calculated [45] by using the following equations [45]:

$$fk^{-} = [q_k(N) - q_k(N-1)] \text{ for an electrophilic attack,} \quad (3)$$

$$fk^{+} = [q_k(N+1) - q_k(N)] \text{ for a nucleophilic attack.} \quad (4)$$

3. Results and Discussion

3.1. Inhibitor Characterization. Figure 2 shows the infrared spectra for the metal complex and the materials used for its synthesis (dibutyltin oxide and curcumin). The different absorption peaks for the carbonyl groups are observed. Hence, the absorption peaks for the carbonyl groups present in the curcumin are shown at 1601 and 1625 cm^{-1}, while these groups were shifted towards lower wave numbers (1588 and 1617 cm^{-1}) for the metallic complex. Thus, it was noticed that the bonding of the tin metal centre to the curcumin carbonyl groups made the carbon-oxygen double bond weaker due to the formation of the metallic complex. The ^{1}H NMR spectrum for the obtained metallic complex is shown in Figure 3. The signal for H1 was shifted to $\delta = 5.7$ ppm as a double as a consequence of the tin coordination; this signal was observed as a singlet for free curcumin. The H3 signal is observed at $\delta = 6.32$ ppm as a double because of the coupling with H4. The aromatic part shows signals at the lower field; for instance, the signal for H6 is shifted to $\delta = 6.90$ ppm as a singlet, H10 is shifted to $\delta = 6.96$ ppm as a doublet, and H9 is shifted to $\delta = 6.78$ ppm. These values are similar to those observed for curcumin because the interaction of the tin atom is carried out in the carbonyl groups. The remaining signals of the hydrogens correspond to the observed hydrogens to the butyl groups. A summary of the shift and constant coupling of the hydrogen atoms for the metallic complex is shown in Table 1. Finally, the mass spectrum of the metallic complex is shown in Figure 4, where it can be seen that the molecular weight corresponding to this complex $m/z = 969$ g/mol was not observed. However, some fragments were detected due to the presence of tin. For instance, a peak in $m/z = 763$ was assigned to the breaking of a curcumin molecule, and the most abundant peak was observed at 307 which is the curcumin molecule with the loss of the methoxy groups.

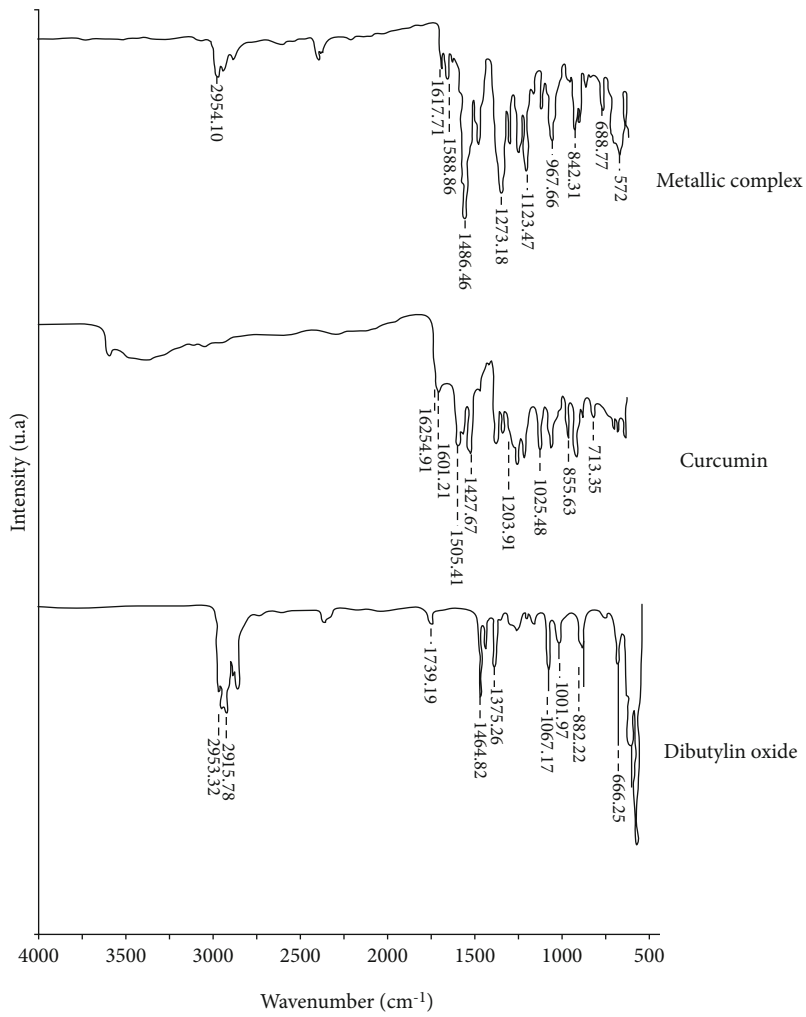

Figure 2: FTIR spectra of curcumin, dibutyltin oxide, and the obtained Sn-metallic complex.

3.2. Weight Loss Tests. The effect of the Sn-metallic complex on the weight loss, inhibitor efficiency, and steel surface area covered by the inhibitor θ (which is the inhibitor efficiency divided by 100) for 1018 carbon steel immersed in 0.5 M H_2SO_4 solution is given in Table 2. In all cases, it is evident that the inhibitor efficiency increases with its concentration, which is due to the adsorption of the metallic complex on the steel surface. The fact that the metal surface area covered by the inhibitor θ increases with its concentration supports the idea that the decrease in the corrosion rate is due to the inhibitor adsorption on the steel surface to form a protective corrosion product film due to the existence of heterocyclic compounds in the inhibitor such as shown in Figure 1 [18–21]. A visual examination of the specimen corroded without an inhibitor showed a severely corroded steel, whereas the corrosion in the presence of an inhibitor corrosion rate of 100 ppm was visibly reduced because of the formation of protective corrosion products on top of the steel surface.

The Sn-metallic complex reduces the steel corrosion rate due to its adsorption onto the steel surface. The interaction between the inhibitor molecules and the steel surface is provided by the adsorption isotherms. As indicated above, it is assumed that θ is related to the inhibitor efficiency, which was obtained from the weight loss experiments. Different adsorption models exist, including the Langmuir, Temkin, Frumkin and Flory-Huggins. As can be seen from Figure 5, the adsorption Frumkin isotherm had the best data fit, with an $R^2 = 0.89$, which is given by

$$\frac{\theta}{(1-\theta)e^{-2f\theta}} = K_{\text{ads}} C_{\text{inh}}, \tag{5}$$

where C_{inh} is the inhibitor adsorption, K_{ads} is the adsorption isotherm, and f is the interaction coefficient, which is positive for attraction and negative for repulsion. The adsorption constant, K_{ads}, and the standard free energy of adsorption (ΔG_{ads}) are related according to the following equation:

$$\Delta G_{\text{ads}} = -RT \ln (106 K_{\text{ads}}), \tag{6}$$

where R is the universal gas constant and T is the absolute temperature. From Figure 5, Frumkin constants were $f = 1719.7$, $K_{\text{ads}} = 33860$ L/mol, and $\Delta G_{\text{ads}} = -25.85$ kJ/mol. The

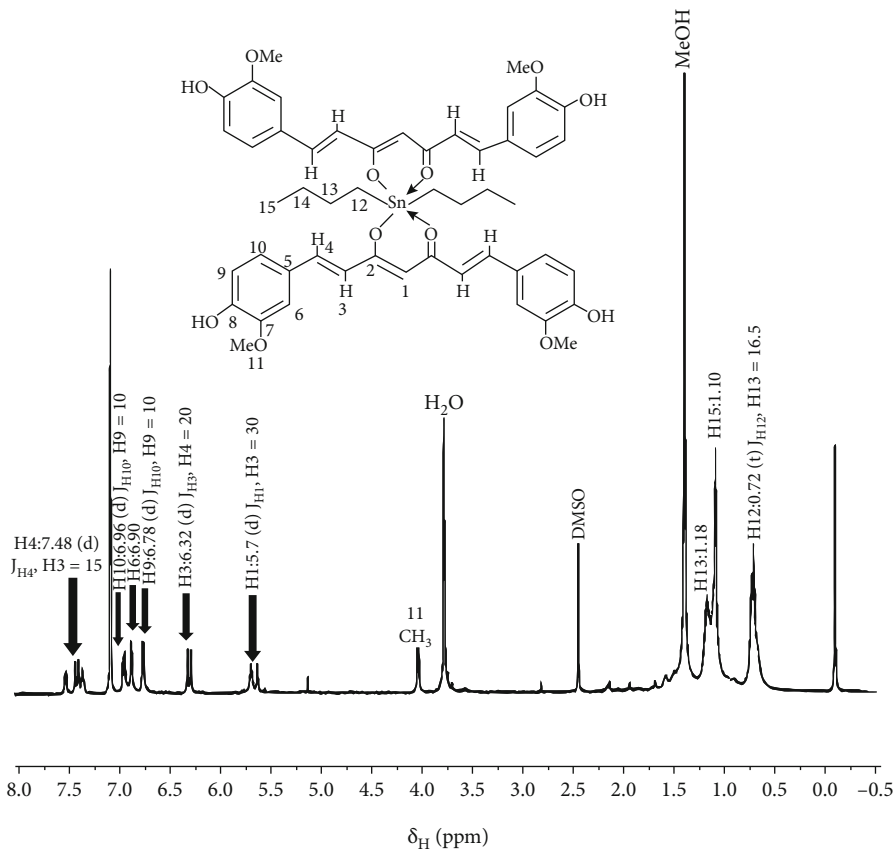

Figure 3: ^{1}H NMR spectrum in DMSO d_6 for the Sn-metallic complex.

Table 1: ^{1}H NMR in DMSO d_6 for the Sn-metallic complex.

H(δ)	H1 : 5.7(d)	H3 : 6.3(d)	H4 : 7.4(d)	H6 : 6.90	H9 : 6.7(d)	H10:6.9(d)	H13 : 1.18	H15 : 1.10	H12 : 0.7(t)
J (Hz)	$J_{H1,H3=20}$	$J_{H3,H4=20}$	$J_{H4,H3=15}$		$J_{H,H10=10}$	$J_{H10,H9=10}$			$J_{1H12,H13=16.5}$

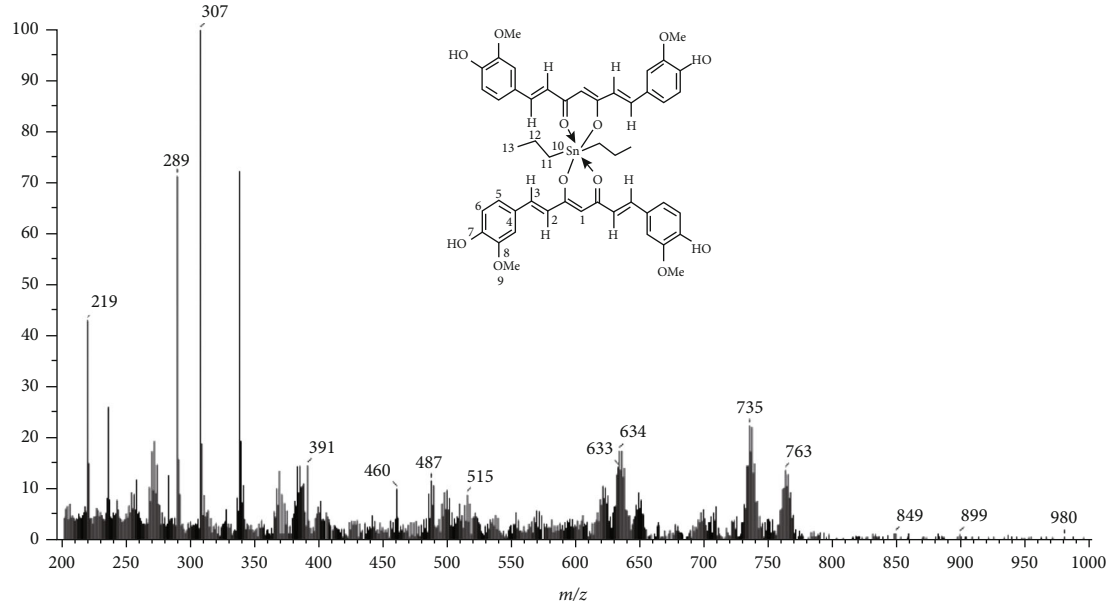

Figure 4: Mass spectrum for the Sn-metallic complex.

Table 2: Effect of the Sn-metallic complex on the weight loss, inhibitor efficiency, and steel surface area covered by the inhibitor, θ, for carbon steel immersed in 0.5 M H_2SO_4.

C_{inh} (ppm)	ΔW (mg/cm^2)	I.E.	θ
0	102.7	—	—
100	16.1	80.5	0.805
200	13.1	82.1	0.821
400	10.8	84.2	0.842
600	2.1	85.3	0.853
800	1.6	87.2	0.872
1000	1.1	89.1	0.891

positive value for f indicates that there is an attraction between the steel surface and the inhibitor, whereas the relatively low value for K_{ads} indicates a weak interaction between the inhibitor molecules and the steel surface; on the other hand, the negative value for ΔG_{ads} indicates a spontaneous process. The ΔG_{ads} value of -25.85 indicates that the type of adsorption between inhibitor molecules and the steel surface is weak and physical in nature, which involves electrostatic interaction between the inhibitor and the charged metal surface [46–48].

3.3. Polarization Curves. Figure 6 displays the polarization curves for 1018 carbon steel immersed in 0.5 M H_2SO_4 solution containing different concentrations of the Sn-containing metallic complex as a corrosion inhibitor. Various parameters such as E_{corr}, I_{corr}, anodic, and cathodic Tafel slopes (β_a and β_c) are reported in Table 3. It is clear that in all cases, regardless the inhibitor concentration, the addition of the Sn-metallic complex results in a marked decrease in both cathodic and anodic current density values, but in a more marked way for the cathodic one. Alternatively, polarization curves displayed an active behaviour, without evidence of the formation of a passive layer. In the cathodic region, there is no clear differentiation between the two cathodic oxygen reduction and hydrogen evolution reactions. However, both cathodic reactions can be clearly differentiated with the addition of the inhibitor. The E_{corr} value was only marginally affected, since it fluctuated between -460 and -480 mV as shown in Table 3. Both anodic and cathodic Tafel slopes were affected by the addition of the inhibitor, thus confirming that the Sn-containing metallic complex is acting as a mixed type of corrosion inhibitor, affecting, therefore, both oxygen reduction and hydrogen evolution reactions. Thus, we can say that the cathodic reactions are retarded by blocking the active sites of the steel where oxygen and hydrogen can be adsorbed, whereas the anodic reaction is retarded by the formation of iron complexes due to the presence of a long pair of electrons in the organic compound structure [49–51].

On the other side, the I_{corr} value was dramatically decreased with the addition of 1000 ppm of inhibitor for almost two orders of magnitude. Inhibitor efficiency was calculated by using:

$$\text{I.E.} = \frac{I_{corr} - I_{corr/inh}}{I_{corr}} \times 100, \quad (7)$$

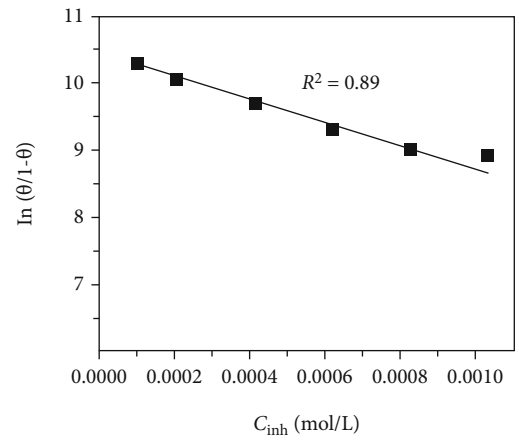

Figure 5: Frumkin type of adsorption isotherm for 1018 carbon steel immersed in 0.5 M H_2SO_4 in the presence of a Sn-metallic complex as corrosion inhibitor.

where I_{corr} and $I_{corr/inh}$ are the corrosion current density values obtained in the absence and presence of the inhibitor, respectively. From the data given in Table 3, we can see that inhibitor efficiency increases with an increase in the inhibitor concentration; its highest value was reached with the addition of 1000 ppm of inhibitor, which indicates that more inhibitor molecules are adsorbed onto the steel surface with an increase in the metal surface area covered by the inhibitor.

3.4. EIS Results. The corrosion behaviour of carbon steel in sulfuric acid with and without the presence of the Sn-containing metallic complex was studied with the aid of EIS studies, and the obtained results are shown in Figure 7. It can be seen that Nyquist diagrams display a single, depressed, and capacitive semicircle at high and intermediate frequency values, followed by an inductive loop at lower frequency values for inhibitor concentrations lower than 800 ppm. The presence of an inductive loop indicates that the corrosion process is controlled by the adsorption/desorption of some intermediate species on the steel surface. On the other hand, for an inhibitor concentration of 1000 ppm, Nyquist data display a capacitive loop at high and intermediate frequency values, followed by an increase in the real impedance value while the imaginary values remain constant at lower frequency values, which is due to the accumulation of all kinds of species at the metal/solution interface and increases the total impedance value [52, 53]. The presence of the capacitive loop at high frequency values indicates that the corrosion of carbon steel in sulfuric acid is mainly controlled by the charge transfer and the formation of a protective film on the steel surface. The imperfect semicircle is generally attributed to the frequency dispersion as a result of roughness of the metal surface, grain boundaries, impurities, and distribution of surface active sites. The shape of the loops was not altered by the addition of the metallic complex, which indicates that this inhibitor reduces the steel corrosion rate without affecting the corrosion mechanism. On the other hand, Bode diagrams, Figure 7(b), showed a single peak and, thus, one time constant only, for the uninhibited

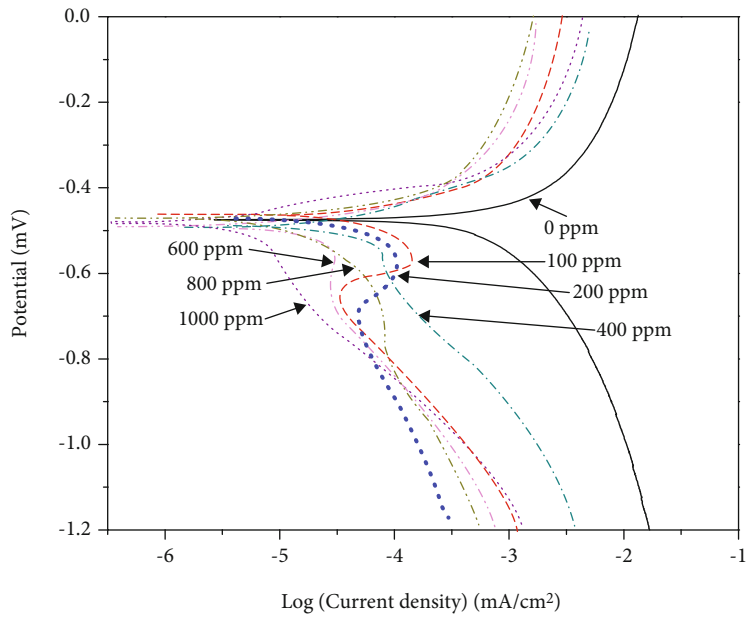

Figure 6: Effect of the Sn-metallic complex concentration on the polarization curves for 1018 carbon steel immersed in 0.5 M H_2SO_4.

Table 3: Electrochemical parameters obtained from polarization curves for carbon steel immersed in 0.5 M H_2SO_4 at different concentrations of Sn-metallic complex.

C_{inh} (ppm)	E_{corr} (mV)	I_{corr} (μA/cm^2)	β_a (mV/dec)	$-\beta_c$ (mV/dec)	I.E. (%)
0	-470	1.04	290	-362	—
100	-460	1.81×10^{-1}	158	-340	82
200	-460	1.12×10^{-1}	111	-288	89
400	-480	1.11×10^{-1}	76	-266	89
600	-480	5.49×10^{-2}	65	-235	94
800	-460	2.51×10^{-2}	48	-207	97
1000	-470	9.54×10^{-3}	16	-180	99

solution and inhibitor concentrations lower than 800 ppm, whereas at an inhibitor concentration, this peak is broadened to a wider frequency interval, indicating the presence of two time constants, due to the presence of a protective corrosion product film.

All EIS spectra were analysed by fitting the experimental data to an appropriate equivalent electric circuit to find the parameters, which are described as being consistent with the experimental data. Figure 8 depicts the proposed electric circuits used to simulate the EIS data. In this figure, R_s is the solution resistance, R_{ct} is the charge transfer resistance, CPE_{dl} is a constant phase element related to the double electrochemical impedance, R_f is the resistance of the film formed by the corrosion products, CPE_f is the constant phase element related to its capacitance, L is the inductive element, and R_L is its resistance. CPE_{dl} and CPE_f are placed instead of an ideal double layer capacitor, C_{dl}, and film capacitance, C_f, to take into account the dispersion effects due to surface roughness and other surface heterogeneities as mentioned above. The impedance of the CPE, Z_{CPE}, is given by [54]

$$Z_{CPE} == \frac{1}{Y_0(i\omega)^n}, \tag{8}$$

where Y_0 is the admittance, $i = -1^{1/2}$, ω the angular frequency, and n a physical parameter which gives interphase properties of the working electrode such as roughness and inhibitor adsorption. Resulting parameters from the use of circuits given in Figure 8 are shown in Table 4. Data given in this table show that the charge resistance value, R_{ct}, increases whereas the CPE_{dl} value decreases with an increase in the inhibitor concentration. Results given in Table 4 are in complete agreement with the weight loss and polarization data, Tables 2 and 3, respectively. An increase in R_{ct} is normally associated with a decrease of the dissolution of the steel because the Sn-metallic complex is adsorbed on its surface by a gradual displacing of the water molecules and the formation of a protective film. This film will isolate the steel surface from the electrolyte and decrease its dissolution rate. Alternatively, the decrease in the CPE_{dl} value is attributed to a lowering in the dielectric constant value, ε, which is caused by the adsorption of the inhibitor molecules which have a lower local dielectric constant value or to the increase in the double electric layer thickness [55] according to the expression of the Helmholtz model for the calculation of the double electric layer capacitance, C_{dl}:

$$C_{dl} = \frac{\varepsilon\varepsilon_0 A}{\delta}, \tag{9}$$

where ε_0 is the vacuum electrical permittivity, δ the electric layer thickness, and A the surface area.

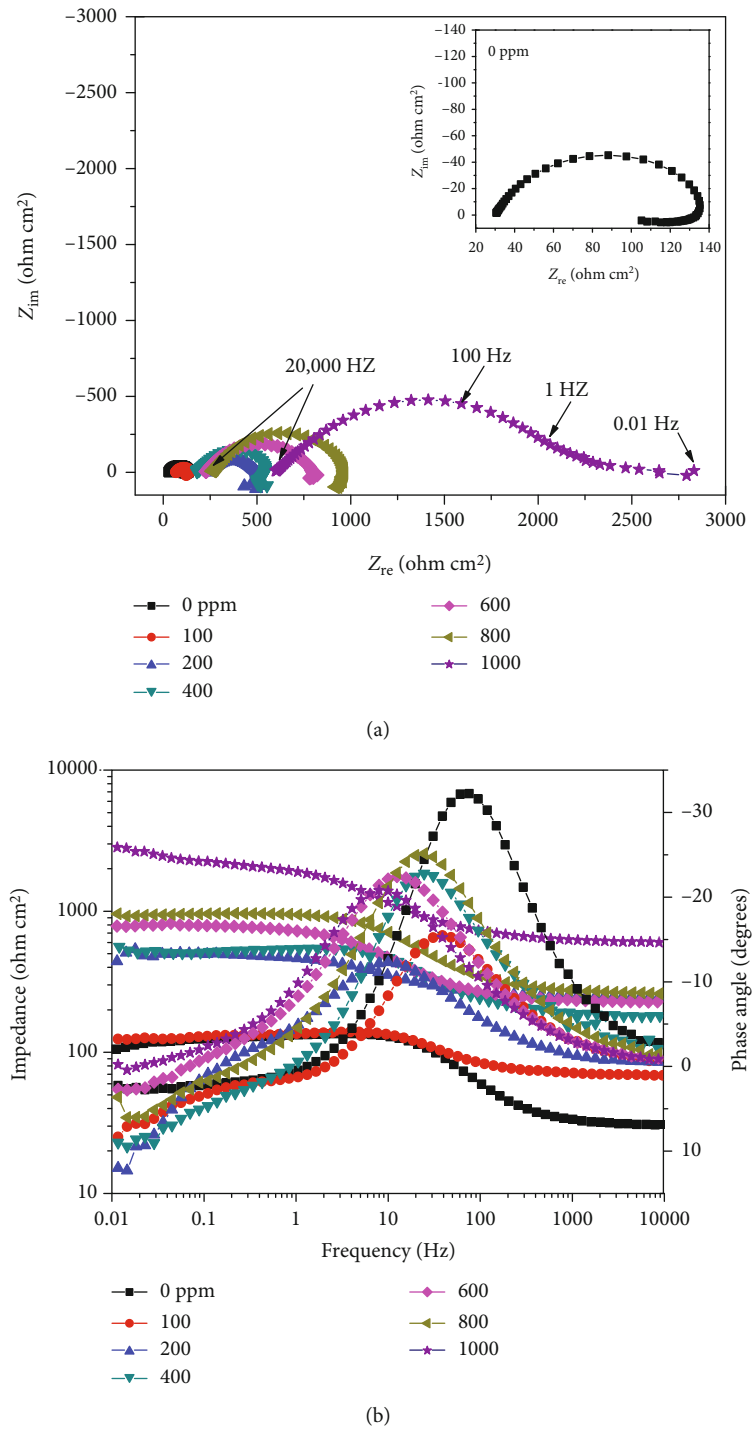

Figure 7: Effect of the Sn-metallic complex concentration on the (a) Nyquist and (b) Bode plots for 1018 carbon steel immersed in 0.5 M H_2SO_4.

3.5. Surface Characterization. After corrosion tests, surfaces were analysed with a scanning electronic microscope, SEM, and micrographs of corroded specimens in the absence and presence of inhibitor are shown in Figure 9. It can be seen that the corrosion product film formed in the absence of an inhibitor, Figure 9(a), shows porous microcracks and some other defects which do not prevent the contact between the electrolyte and the steel. Unlike this, the formed film in the presence of the inhibitor, Figure 9(b), is much more compact, with a much lower amount of porous and microcracks, avoiding the contact between the corrosive solution and the steel surface.

3.6. Quantum Chemical Calculations

3.6.1. Neutral Molecule. The optimized structure of the molecule in its neutral state is shown in Figure 10. As it is

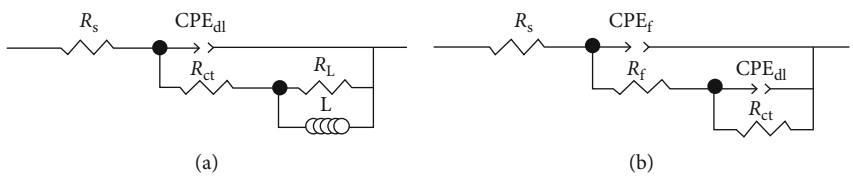

Figure 8: Electric circuits to simulate EIS data for 1018 carbon steel immersed in 0.5 M H_2SO_4 in the presence of the Sn-metallic complex in concentrations of (a) lower than 800 ppm and (b) 1000 ppm.

Table 4: Electrochemical parameters used to simulate EIS data for carbon steel immersed in 0.5 M H_2SO_4 at different concentrations of Sn-metallic complex.

C_{inh} (ppm)	CPE_{dl} ($\mu Ss^n/cm^2$)	n	R_{ct} (ohm cm^2)	CPE_f ($\mu Ss^n/cm^2$)	n_f	R_f (ohm cm^2)	R_L (ohm cm^2)
0	2.2×10^{-4}	0.7	96	—	—	—	16.24
100	1.19×10^{-4}	0.8	102	—	—	—	17.56
200	9.5×10^{-5}	0.8	387	—	—	—	159.1
400	7.3×10^{-5}	0.8	542	—	—	—	104.9
600	4.9×10^{-5}	0.8	555	—	—	—	119.3
800	1.2×10^{-5}	0.8	900	—	—	—	214.9
1000	8.5×10^{-6}	0.9	1962	8.5×10^{-3}	0.9	780	—

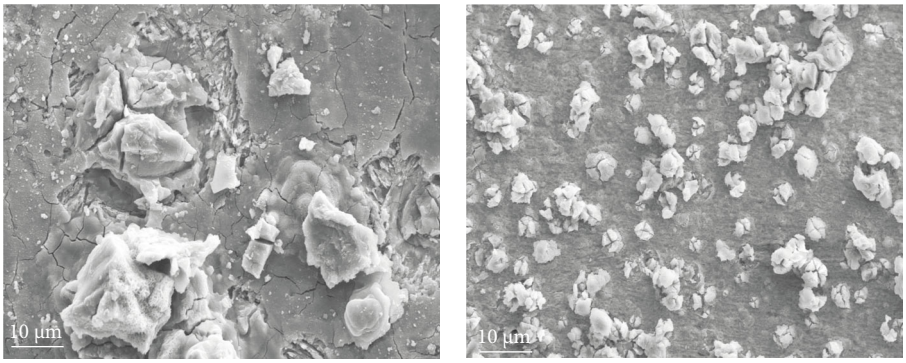

Figure 9: SEM micrographs of corroded 1018 carbon steel in 0.5 M H_2SO_4 in the presence of (a) 0 and (b) 1000 ppm of the Sn-metallic complex.

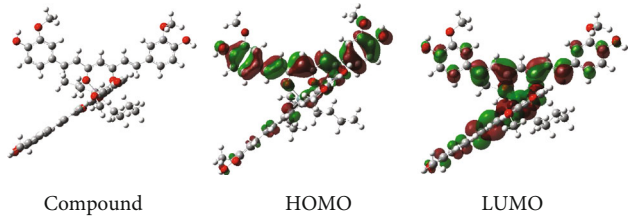

Figure 10: Optimized molecular structure and HOMO and LUMO orbitals of the Sn-metallic complex, SnX molecule. Atomic colours represent gray (C), white (H), red (O), blue (N), and dark-blue-square (Sn).

assumed that the inhibitor is most likely to be an electron donor with respect to the metallic surface, the electron density distribution of the HOMO is of particular significance [56]. The HOMO and LUMO orbital distributions of the Sn-metallic complex, which we will call the SnX molecule from now on, are shown in Figure 10. Table 5 indicates that the negative value of HOMO for the Sn-containing metallic complex indicates a greater efficiency of inhibition of the compound. The hardness obtained value for the SnX is an important property to measure molecular stability, and inhibition of a molecule was 1.33 eV. Furthermore, the value for the dipolar moment is an important indicator which had a value of 13.02 for SnX also. Electrophilicity, ω, on the other hand, denotes the electron-accepting capability of the molecule where a value of 6.97 eV was obtained. Table 5 gives data for parameters such as IP, EA, χ, and η [57, 58]. Further analysis of Fukui functions of the SnX molecule are shows in Figure 11 indicating that there is a nucleophilic attack in the C41 atom whereas the electrophilic attack occurs in the O10 atom. It has been found that the sites with electrophilic attack are places with enhanced HOMO energies; conversely, LUMO sites are most susceptible to suffer nucleophilic attack [57].

Table 5: The calculated quantum chemical descriptors for the metallic complex, SnX molecule, obtained using DFT at the B3LYP/LANL2DZ basis set in aqueous phase.

Neutral molecule	HOMO (eV)	LUMO (eV)	ΔE (eV)	μ (Debye)	IP (eV)	EA (eV)	χ (eV)	η (eV)	ω (eV)
	-5.77	-2.79	2.79	13.02	5.64	2.98	4.31	1.33	6.97

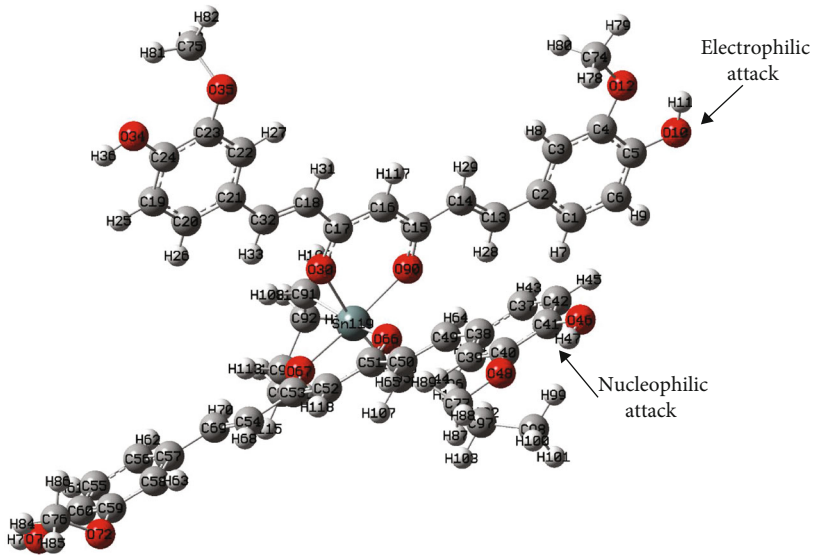

Figure 11: Fukui function distribution for electrophilic attack and nucleophilic attack for the Sn-metallic complex, SnX molecule.

Table 6: The calculated quantum chemical descriptors for protonated SnX molecule obtained using DFT at the B3LYP/LANL2DZ basis set in aqueous phase.

Protonated molecule	HOMO (eV)	LUMO (eV)	ΔE (eV)	μ (Debye)	IP (eV)	EA (eV)	χ (eV)	η (eV)	ω (eV)
	-5.80	-2.96	3.43	38.03	5.68	3.12	4.40	1.28	7.58

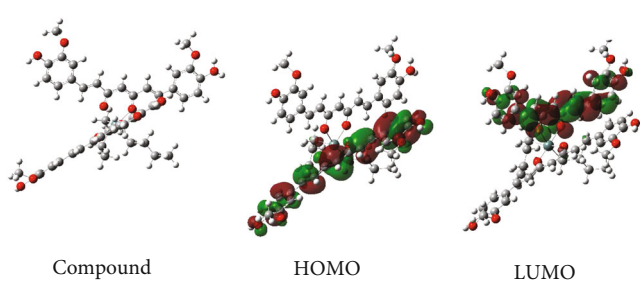

Figure 12: Optimized molecular structure of protonated SnX molecule and HOMO and LUMO orbitals of the Sn-metallic complex, SnX molecule. Atomic colours represent gray (C), white (H), red (O), blue (N), and dark-blue-square (Sn).

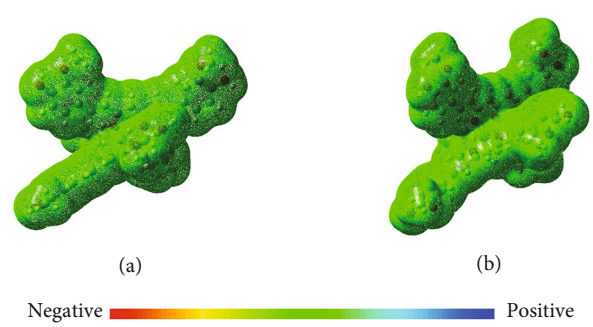

Figure 13: The calculated molecular electrostatic potential (MEP) map: the colour range (blue more positive, red more negative) oscillates for (a) neutral SnX, -1.041e-1 from 1.041e-1, and (b) protonated SnX, -9.952 from 9.952. Atomic colours represent gray (C), white (H), red (O), blue (N), and dark-blue-square (Sn).

3.6.2. Protonated Molecule. The optimized structure of the SnX molecule in its neutral state contains more than one active centre for protonation according to the electronic density observed in HOMO that corresponds of the electrophilic attack (Figure 11). Thus, the protonation site of the molecule was determined through the Fukui functions. According to the Fukui function, the most susceptible site for an electrophilic attack in the SnX molecule is located on the O10 atom. Once the molecules are protonated, the electronic parameters of the protonated inhibitor molecule such as HOMO, LUMO, ΔE, dipole moment, and reactivity parameters are shown in Table 6. Additionally, the optimized structure, HOMO, and LUMO are shown in Figure 12. The HOMO value of the protonated SnX molecule is -5.80 eV. The dipolar moment value, μ, in the protonated inhibitor had a value of 38.03 Debye. The electronegativity value, χ, measures the

capacity of an atom to attract electrons [58] which is commonly considered in corrosion studies. Therefore, high values of χ indicate better attraction properties, and that value for the protonated SnX molecule was 4.40 eV; according to Kaya et al. [59], electronegativity is one of the parameters that provide important clues about corrosion inhibition efficiency of any chemical species. On the other hand, Figure 13 shows the molecular electrostatic potential (MEP) of the neutral and protonated molecules, where it can be seen that all molecules have a green region, namely, both molecules are in the intermediate zone of the electrostatic potential.

4. Conclusions

A Sn-containing metallic complex derived from *Curcuma longa*, bis[1,7-bis(4-hydroxy-3-methoxyphenyl)-1,6-heptadiene-3,5-dionato-κO,κO′]bis(butyl), was evaluated as a green corrosion inhibitor for 1018 carbon steel in sulfuric acid. Adsorption of the metallic complex corrosion inhibitor produced a decrease in the corrosion rate of steel, and it was found to follow the Frumkin adsorption isotherm. The metallic complex affects the kinetics of the corrosion processes, and its inhibition efficiencies increased with an increase in the inhibitor concentration. Thermodynamic parameters revealed that the inhibitor is spontaneously adsorbed. Negative values for ΔG_{ads} indicate a spontaneous adsorption process of this metallic complex on to the steel surface. SEM analysis showed that the inhibition of corrosion by the Sn-metallic complex is due to the formation of a physically adsorbed film constituted by inhibitor molecules and corrosion products on the metal surface. Theoretical calculations demonstrated the relationship between inhibitor efficiency and its electronic properties.

Data Availability

There is no data availability.

Conflicts of Interest

The authors declare that they have no conflicts of interest.

References

[1] M. Abd El-Raouf, E. A. Khamis, T. H. Maram, and N. A. Negm, "Electrochemical and quantum chemical evaluation of new bis (coumarins) derivatives as corrosion inhibitors for carbon steel corrosion in 0.5 M H_2SO_4," *Journal of Molecular Liquids*, vol. 255, pp. 341–353, 2018.

[2] G. Babaladimath, V. Badalamoole, and S. T. Nanibewoor, "Electrical conducting xanthan gum-graft-polyaniline as corrosion inhibitor for aluminum in hydrochloric acid environment," *Materials Chemistry and Physics*, vol. 205, pp. 171–179, 2018.

[3] S. Bashir, V. Sharma, H. Lgaz, I.-M. Chung, A. Singh, and A. Kumar, "The inhibition action of analgin on the corrosion of mild steel in acidic medium: a combined theoretical and experimental approach," *Journal of Molecular Liquids*, vol. 263, pp. 454–462, 2018.

[4] A. Kahyarian, A. Schumaker, B. Brown, and S. Nesic, "Acidic corrosion of mild steel in the presence of acetic acid: mechanism and prediction," *Electrochimica Acta*, vol. 258, pp. 639–652, 2017.

[5] M. Chellouli, D. Chebabe, A. Dermaj et al., "Corrosion inhibition of iron in acidic solution by a green formulation derived from Nigella sativa L," *Electrochimica Acta*, vol. 204, pp. 50–59, 2016.

[6] G. Gece, "Drugs: a review of promising novel corrosion inhibitors," *Corrosion Science*, vol. 53, no. 12, pp. 3873–3898, 2011.

[7] M. N. Kakadei and J. Neshati, "Corrosion inhibition of carbon steel in diethanolamine–H_2O–CO_2 system by some organic sulphur compounds," *Corrosion Engineering Science and Technology*, vol. 54, no. 3, pp. 413–421, 2019.

[8] R. N. Patel, "Structural, magnetic and spectroscopic characterization of two unusual end-on bis(l-acetato/l-nitrato) bridged copper(II) complexes with N0-[phenyl(pyridin-2-yl) methylidene]furan-2-carbohydrazide and (2E,4Z)-N,2dimethylhepta-2,4,6- trienamide-1-phenyl-1-pyridin-2ylmethanimine (1:1) as capping ligands," *Inorganic Chemistry Acta*, vol. 363, pp. 3838–3846, 2010.

[9] C. Monticelli, A. Balbo, J. Esvan et al., "Evaluation of 2-(salicylideneimino) thiophenol and other Schiff bases as bronze corrosion inhibitors by electrochemical techniques and surface analysis," *Corrosion Science*, vol. 148, pp. 144–158, 2019.

[10] M. K. Bagga, R. Gadi, O. S. Yadav, R. Kumar, R. Chopra, and G. Singh, "Investigation of phytochemical components and corrosion inhibition property of Ficus racemose stem extract on mild steel in H_2SO_4 medium," *Journal of Environmental Chemical Engineering*, vol. 4, no. 12, pp. 4699-4700, 2016.

[11] V. S. Helbert, L. Gaillet, T. Chaussadent, V. Gaudefroy, and J. Creus, "Rhamnolipids as an eco-friendly corrosion inhibitor of rebars in simulated concrete pore solution: evaluation of conditioning and addition methods," *Corrosion Engineering Science and Technology*, vol. 55, no. 2, pp. 91–102, 2019.

[12] Z. V. P. Murthy and K. Vijayaragavan, "Mild steel corrosion inhibition by acid extract of leaves of Hibiscus sabdariffa as a green corrosion inhibitor and sorption behavior," *Green Chemistry Letters and Reviews*, vol. 7, no. 2, pp. 209–219, 2014.

[13] G. Khan, K. M. Newaz, W. J. Basirun, H. B. Ali, F. L. Faraj, and G. M. Khan, "Application of natural product extracts as green corrosion inhibitors for metals and alloys in acid pickling processes - a review," *International Journal of Electrochemical Science*, vol. 10, no. 6, pp. 6120–6134, 2015.

[14] R. Haldhar, D. Prasad, and A. Saxena, "Myristica fragrans extract as an eco-friendly corrosion inhibitor for mild steel in 0.5M H_2SO_4 solution," *Journal of Environmental Chemical Engineering*, vol. 6, no. 11, pp. 2290–2301, 2018.

[15] H. Ashassi-Sorkhabi, S. Mirzaee, T. Rostamikia, and R. Bagheri, "Pomegranate (Punica granatum) peel extract as a green corrosion inhibitor for mild steel in hydrochloric acid solution," *International Journal of Corrosion*, vol. 2015, Article ID 197587, 6 pages, 2015.

[16] M. Hazwan Hussin, A. A. Rahim, M. N. M. Ibrahim, and N. Brosse, "Improved corrosion inhibition of mild steel by chemically modified lignin polymers from Elaeis guineensis agricultural waste," *Materials Chemistry and Physics*, vol. 163, pp. 201–212, 2015.

[17] A. Singh, V. K. Singh, and M. A. Quraishi, "Aqueous extract of Kalmegh (Andrographis paniculata) leaves as green inhibitor for mild steel in hydrochloric acid solution," *International*

Journal of Corrosion, vol. 2010, Article ID 275983, 10 pages, 2010.

[18] E. M. Tanvir, M. Hossen, M. Hossain et al., "Antioxidant properties of popular turmeric (Curcuma longa) varieties from Bangladesh," *Journal of Food Quality*, vol. 2017, Article ID 8471785, 8 pages, 2017.

[19] A. Gupta, S. Mahajan, and R. Sharma, "Evaluation of antimicrobial activity of Curcuma longa rhizome extract against Staphylococcus aureus," *Biotechnology Reports*, vol. 6, no. 1, pp. 51–55, 2015.

[20] S. Y. Park and D. S. H. L. Kim, "Discovery of natural products from Curcuma longa that protect cells from beta-amyloid insult: a drug discovery effort against Alzheimer's disease," *Journal of Natural Products*, vol. 65, no. 10, pp. 1227–1231, 2002.

[21] T. T. Dao, P. H. Nguyen, H. K. Won, E. H. Kim, J. Park, and B. Y. Won, "Curcuminoids from Curcuma longa and their inhibitory activities on influenza A neuraminidases," *Food Chemistry*, vol. 134, pp. 21–28, 2012.

[22] V. Johnsirani, S. Rajendran, A. Christy, and C. Mary, "Corrosion inhibition by dyes from plants," *International Journal of Nano Corrosion Science and Engineering*, vol. 2, no. 1, pp. 22–28, 2015.

[23] R. M. A. Shahba, A. E. E. Fouda, A. E. El-Shenawy, and A. S. M. Osman, "Effect of Catharanthus roseus (Vince rosea) and turmeric (Curcumalonga) extracts as green corrosion inhibitors for mild steel in 1 M HCl," *Materials Science and Applications*, vol. 7, no. 5, pp. 654–671, 2016.

[24] N. I. Kairi and J. Kassim, "The effect of temperature on the corrosion inhibition of mild steel in 1 M HCl solution by Curcuma longa extract," *International Journal of Electrochemical Science*, vol. 8, no. 6, pp. 7138–7155, 2013.

[25] A. M. Al-Fakih, M. Aziz, and H. M. Sirat, "Turmeric and ginger as green inhibitors of mild steel corrosion in acidic medium," *Journal of Materials and Environmental Science*, vol. 6, no. 10, pp. 1480–1487, 2015.

[26] A. S. Fouda and K. M. Elattar, "Curcumin derivatives as green corrosion inhibitors for a-Brass in nitric acid solution," *Journal of Materials Engineering and Performance*, vol. 21, no. 10, pp. 2354–2362, 2012.

[27] S. Rajendran, K. Duraiselvi, P. Prabhakar, M. Pandiarajan, M. Tamilmalar, and R. J. Rathish, "Corrosion resistance of Al in simulated concrete pore solution in the presence of curcumin extract," *European Chemical Bulletin*, vol. 2, no. 6, pp. 850–854, 2013.

[28] D. Kandias, B. Bundjali, and D. Wahyuningrum, "Curcuminoid compounds isolated from Curcuma domestica Val. as corrosion inhibitor towards carbon steel in 1% NaCl solution," *Sains Malaysiana*, vol. 40, no. 8, pp. 1013–1018, 2011.

[29] E. A. Flores-Frias, V. Barba, M. A. Lucio-Garcia, R. Lopez-Cecenes, J. Porcayo-Calderon, and J. G. Gonzalez-Rodriguez, "Use of Curcuma and curcumin as a green corrosion inhibitors for carbon steel in sulfuric acid," *International Journal of Electrochemical Science*, vol. 14, no. 10, pp. 5026–5041, 2019.

[30] K. I. Priyadarsini, "The chemistry of curcumin: from extraction to therapeutic agent," *Molecules*, vol. 19, pp. 20091–20112, 2014.

[31] M. J. Frisch, G. W. Trucks, H. B. Schlegel et al., *Gaussian 09, Revision A. 01 Gaussian*, Wallingford, CT, 2009.

[32] W. Kohn and L. J. Sham, "Self-consistent equations including exchange and correlation effects," *Physics Review*, vol. 140A, pp. A1133–A1138, 1965.

[33] G. Robert and W. Y. Parr, *Density-Functional Theory of Atoms and Molecules*, Oxford University Press, New York, USA, 1989.

[34] W. Kohn and P. Hohenbergt, "Inhomogeneous electron gas," *Physics Review*, vol. 136B, pp. B864–B871, 1964.

[35] A. D. Becke, "Density-functional thermochemistry. III. The role of exact exchange," *Journal of Chemical Physics*, vol. 98, no. 9, pp. 5648–5652, 1993.

[36] P. J. Hay and W. R. Wadt, "Ab initio effective core potentials for molecular calculations - potentials for the transition-metal atoms Sc to Hg," *Journal of Chemical Physics*, vol. 82, no. 2, pp. 270–283, 1985.

[37] W. R. Wadt and P. J. Hay, "Ab initio effective core potentials for molecular calculations - potentials for main group elements Na to Bi," *Journal of Chemical Physics*, vol. 82, no. 2, pp. 284–298, 1985.

[38] P. J. Hay and W. R. Wadt, "Ab initio effective core potentials for molecular calculations - potentials for K to Au including the outermost core orbitals," *Journal of Chemical Physics*, vol. 82, no. 2, pp. 299–310, 1985.

[39] C. Amovilli, V. Barone, R. Cammi, E. Cancès, M. Cossi, and B. Mennucci, *Recent advances in the description of solvent effects with the polarizable continuum model*, P.-O. Löwdin, Ed., vol. 32, Academic Press, 1998.

[40] B. Mennucci, E. Cancès, and J. Tomasi, "Evaluation of solvent effects in isotropic and anisotropic dielectrics and in ionic solutions with a unified integral equation method: theoretical bases, computational implementation, and numerical applications," *The Journal of Physical Chemistry B*, vol. 101, pp. 10506–10517, 1997.

[41] R. G. Pearson, "Hard and soft acids and bases," *Journal of the American Chemical Society*, vol. 85, pp. 3533–3539, 1963.

[42] R. G. Parr, R. A. Donnelly, L. Mel, and W. E. Palke, "Electronegativity: the density functional viewpoint," *Journal of Chemical Physics*, vol. 68, no. 12, pp. 3801–3807, 1978.

[43] P. K. Chattaraj, U. Sarkar, and D. R. Roy, "Electrophilicity index," *Chemical Reviews*, vol. 106, pp. 2065–2091, 2006.

[44] M. V. Putz, N. Russo, and E. Sicilia, "Atomic radii scale and related size properties from density functional electronegativity formulation," *Journal of Physical Chemistry A*, vol. 107, pp. 5461–5465, 2003.

[45] K. Fukui, *Theory of Orientation and Stereo Selection*, Springer-Verlag, New York, 1975.

[46] C. M. Goulart, A. Esteves-Souza, C. A. Martinez-Huitle, C. J. F. Rodrigues, M. A. M. Maciel, and A. Echevarria, "Experimental and theoretical evaluation of semicarbazones and thiosemicarbazones as organic corrosion inhibitors," *Corrosion Science*, vol. 67, no. 2, pp. 281–291, 2013.

[47] M. A. Amin and M. M. Ibrahim, "Corrosion and corrosion control of mild steel in concentrated H_2SO_4 solutions by a newly synthesized glycine derivative," *Corrosion Science*, vol. 53, no. 6, pp. 873–885, 2011.

[48] S. Varvara, L. M. Muresan, K. Rahmouni, and H. Takenouti, "Evaluation of some non-toxic thiadiazole derivatives as bronze corrosion inhibitors in aqueous solution," *Corrosion Science*, vol. 50, no. 11, pp. 2596–2604, 2008.

[49] K. Marusic, H. O. Curkovic, and H. Takenouti, "Inhibiting effect of 4-methyl-1-p-tolylimidazole to the corrosion of bronze patinated in sulphate medium," *Electrochimica Acta*, vol. 56, pp. 7491–7502, 2011.

[50] A. B. Nazeer, E. A. Ashour, and N. K. Allam, "Potential of 5-methyl 1-H benzotriazole to suppress the dissolution of α-

aluminum bronze in sulfide-polluted salt water," *Materials Chemistry and Physics*, vol. 144, pp. 55–65, 2014.

[51] X. Li, S. Deng, and H. Fu, "Triazolyl blue tetrazolium bromide as a novel corrosion inhibitor for steel in HCl and H_2SO_4 solutions," *Corrosion Science*, vol. 53, no. 2, pp. 302–309, 2011.

[52] M. Özcan, I. Dehri, and M. Erbil, "Organic sulphur-containing compounds as corrosion inhibitors for mild steel in acidic media: correlation between inhibition efficiency and chemical structure," *Applied Surface Science*, vol. 236, pp. 155–164, 2004.

[53] R. Solmaz, G. Kardas, M. Culha, B. Yazıcı, and M. Erbil, "Investigation of adsorption and inhibitive effect of 2-mercaptothiazoline on corrosion of mild steel in hydrochloric acid media," *Electrochimica Acta*, vol. 53, pp. 5941–5952, 2008.

[54] G. Golestani, M. Shahidi, and D. Ghazanfari, "Electrochemical evaluation of antibacterial drugs as environment-friendly inhibitors for corrosion of carbon steel in HCl solution," *Applied Surface Science*, vol. 308, pp. 347–362, 2014.

[55] Z. El Adnani, M. Mcharfi, M. Sfaira, M. Benzakour, A. T. Benjelloun, and M. E. Touhami, "DFT theoretical study of 7-R-3methylquinoxalin-2 (1H)-thiones (RH; CH3; Cl) as corrosion inhibitors in hydrochloric acid," *Corrosion Science*, vol. 68, no. 2, pp. 223–230, 2013.

[56] A. Zarrouk, H. Zarrok, R. Salghi et al., "A theoretical investigation on the corrosion inhibition of copper by quinoxaline derivatives in nitric acid solution," *International Journal of Electrochemical Science*, vol. 7, no. 11, pp. 6353–6364, 2012.

[57] J. Zhang, G. Qiao, S. Hu, Y. Yan, Z. Ren, and L. Yu, "Theoretical evaluation of corrosion inhibition performance of imidazoline compounds with different hydrophilic groups," *Corrosion Science*, vol. 53, no. 1, pp. 147–152, 2011.

[58] M. Finsgar, A. Lesar, A. Kokalj, and I. Milosev, "A comparative electrochemical and quantum chemical calculation study of BTAH and BTAOH as copper corrosion inhibitors in near neutral chloride solution," *Electrochimica Acta*, vol. 53, pp. 8287–8297, 2008.

[59] S. Kaya, B. Tüzün, C. Kaya, and I. B. Obot, "Determination of corrosion inhibition effects of amino acids: quantum chemical and molecular dynamic simulation study," *Journal of the Taiwan Institute of Chemical Engineers*, vol. 58, no. 3, pp. 528–535, 2016.